

Constitutive behaviors of composites with interface debonding: the extended Mori–Tanaka method for uniaxial tension

Henry Tan · Young Huang · Cheng Liu ·
Guruswami Ravichandran · Glaucio H. Paulino

Received: 28 April 2007 / Accepted: 19 October 2007 / Published online: 13 November 2007
© Springer Science+Business Media B.V. 2007

Abstract Debonding of particle/matrix interfaces can significantly affect the macroscopic behavior of composite materials. We have used a nonlinear cohesive law for particle/matrix interfaces to study the effect of interface debonding on the macroscopic behavior of particle-reinforced composite materials subject to uniaxial tension. The Mori–Tanaka method, which is suitable for composites with high particle volume fraction, is extended to account for interface debonding. At a fixed particle volume fraction, small particles lead to the hardening behavior of the composite while large particles yield softening. The interface sliding may contribute significantly to the macroscopic behavior of the composite.

Keywords Interface debonding · Size effect · Mori–Tanaka method · Composites · Cohesive law

1 Introduction

Debonding of particle/matrix interfaces in composites may significantly affect their macroscopic behavior since interface debonding leads to crack initiation and propagation. Interface debonding is usually characterized by a nonlinear cohesive law (e.g., Needleman 1987; Tvergaard and Hutchinson 1992, 1993; Xu and Needleman 1994; Camacho and Ortiz 1996; Zhong and Knauss 1997, 1999, 2000; Espinosa et al. 1998; Geubelle and Baylor 1998; Huang and Gao 2001; Zhang et al. 2002; Kubair et al. 2002, 2003; Samudrala et al. 2002; Samudrala and Rosakis 2003; Thiagarajan et al. 2004a, b; Tan et al. 2005a, 2006, 2007), which gives the stress tractions in terms of displacement discontinuities across the interface. Tan et al. (2005b) combined experiments and micromechanics models to determine the cohesive law for particle/matrix interfaces in the high explosive PBX 9501. The bilinear interface cohesive law obtained displays three stages, namely the linear debonding (stage-I), softening (stage-II), and complete debonding (stage-III), as illustrated in Fig. 1. The cohesive properties, including the linear modulus, cohesive strength, and softening modulus, have been obtained for PBX 9501. Using such a cohesive law, Tan et al. (2005a, 2006) studied the effect of nonlinear interface debonding on macroscopic constitutive behavior

H. Tan (✉)
School of Mechanical, Aerospace and Civil Engineering,
The University of Manchester, Manchester, M60 1QD UK
e-mail: henry.tan@manchester.ac.uk

Y. Huang
Departments of Civil and Environmental Engineering
and Mechanical Engineering, Northwestern University,
Evanston, IL, 60208 USA
e-mail: huang9@uiuc.edu

C. Liu
Materials Science and Technology Division, Los Alamos
National Laboratory, Los Alamos, NM, 87545 USA

G. Ravichandran
Graduate Aeronautical Laboratory, California Institute
of Technology, Pasadena, CA, 91125 USA

G. H. Paulino
Department of Civil and Environmental Engineering,
University of Illinois, Urbana, IL, 61801 USA

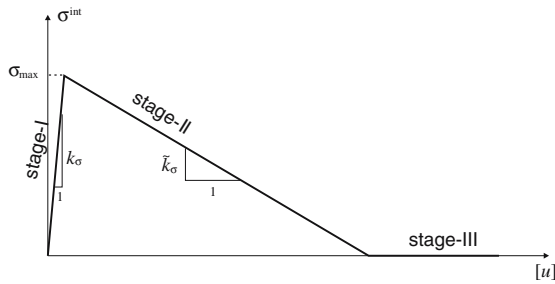


Fig. 1 Three-stage interface cohesive law

of the high explosive PBX 9501 subject to hydrostatic tension. The composite behaves nonlinearly after the interface strength being reached. Small particles lead to hardening behavior of PBX 9501 while large particles yield softening behavior. Large particles may also lead to a sharp stress drop for a composite subject to strain controlled loading.

Recently Tan et al. (2007) studied interface debonding in composites subject to uniaxial tension since it is a widely used test to characterize the material behavior. However, their study is limited to the dilute solution, which neglects the particle–particle interactions and is therefore not suitable for composites with high particle volume fraction such as high explosives (7% binder

2 Previous results

2.1 A cohesive law for particle/matrix interfaces in the high explosive PBX 9501

Interface cohesive law is expressed in terms of traction–displacement relations. Generally, the interface displacement involves both opening and sliding, and the interface traction involves both normal and tangential stresses. Tan et al. (2005b) measured the cohesive law of particle/matrix interfaces for high explosive PBX 9501 subject to increasing hydrostatic tension. Under the hydrostatic tension the interface sliding, and thus the tangential interface traction, can be neglected. As shown in Fig. 1, the cohesive law for an interface with increasing opening $[u]$ is well characterized by three stages, namely the linear debonding, softening, and complete debonding, and each stage gives a straight line. The cohesive law involves three parameters, namely the interface cohesive strength σ_{\max} , linear modulus k that gives the slope of the traction–curve in stage-I of the interface debonding, and softening modulus \tilde{k} that gives the slope in stage-II. These three interface parameters are measured to be $\sigma_{\max} = 1.66$ MPa, $k = 1.55$ GPa/ μm and $\tilde{k} = 17$ MPa/mm for the high explosive PBX 9501 (Tan et al. 2005b). The normal stress at the interface σ^{int} is then related to the opening displacement $[u]$ by

$$\sigma^{\text{int}} = \begin{cases} k[u] & \text{for stage-I, } [u] \leq \sigma_{\max}/k \\ (1 + \tilde{k}/k) \sigma_{\max} - \tilde{k}[u] & \text{for stage-II, } \sigma_{\max}/k < [u] < \sigma_{\max} \left(\frac{1}{k} + \frac{1}{\tilde{k}} \right) \\ 0 & \text{for stage-III, } [u] \geq \sigma_{\max} \left(\frac{1}{k} + \frac{1}{\tilde{k}} \right) \end{cases}, \tag{1}$$

matrix with 93% energetic particles) and solid propellants (more than 60% energetic particles).

We study in this paper the nonlinear interface debonding in composites with high particle volume fraction subject to uniaxial tension. Previous studies on the three-stage interface cohesive law for the high explosive PBX 9501 (Tan et al. 2005b) and a fundamental solution for composites with interface debonding (Tan et al. 2007) are summarized in Sect. 2, based on which the Mori–Tanaka method is extended to account for interface debonding in Sect. 3. Results in Sect. 4 clearly show strong particle size effect, and the interplay between the particle volume fraction and nonlinear interface debonding.

where the bracket $[\]$ is used to denote displacement jump at the interface.

An essential length scale, critical opening displacements of the interface $\delta_{\text{open}} = \sigma_{\max} \left(\frac{1}{\tilde{k}} + \frac{1}{k} \right)$, is introduced, which is $98 \mu\text{m}$ for the high explosive PBX 9501. With the length scale δ_{open} the relation between the normal stress σ^{int} and the opening displacement $[u]$, expressed in Eq. 1, can be reorganized as

$$\frac{\sigma^{\text{int}}}{\sigma_{\max}} = \begin{cases} \frac{1}{\lambda_e} \frac{[u]}{\delta_{\text{open}}} & \text{for stage-I, } \frac{[u]}{\delta_{\text{open}}} \leq \lambda_e \\ \frac{1}{1-\lambda_e} \left(1 - \frac{[u]}{\delta_{\text{open}}} \right) & \text{for stage-II, } \lambda_e < \frac{[u]}{\delta_{\text{open}}} < 1 \\ 0 & \text{for stage-III, } \frac{[u]}{\delta_{\text{open}}} \geq 1 \end{cases}, \tag{2}$$

where the interface elastic limit $\lambda_e = \frac{\tilde{k}}{\tilde{k}+k}$. The integration of the normal stress σ^{int} over the opening displacement $[u]$ gives the cohesive energy

$$\frac{\phi}{\gamma_{\text{int}}} = \begin{cases} \frac{1}{\lambda_e} \left(\frac{[u]}{\delta_{\text{open}}} \right)^2 & \text{for stage-I, } \frac{[u]}{\delta_{\text{open}}} \leq \lambda_e \\ 1 - \frac{1}{1-\lambda_e} \left(1 - \frac{[u]}{\delta_{\text{open}}} \right)^2 & \text{for stage-II, } \lambda_e < \frac{[u]}{\delta_{\text{open}}} < 1, \\ 1 & \text{for stage-III, } \frac{[u]}{\delta_{\text{open}}} \geq 1 \end{cases} \tag{3}$$

where the total interface cohesive energy $\gamma_{\text{int}} = \sigma_{\text{max}}^2 \left(\frac{1}{k} + \frac{1}{\tilde{k}} \right) / 2$.

The above interface cohesive law has been used to study the constitutive behavior of composite materials subject to hydrostatic tension (Tan et al. 2005a, 2006). However, only interface opening displacement is considered in Eqs. 2 and 3. The effect of interface sliding displacement $[v]$ can be accounted for via the combined measure of displacement discontinuity $\lambda = \sqrt{\left(\frac{[u]}{\delta_{\text{open}}} \right)^2 + \left(\frac{[v]}{\delta_{\text{slide}}} \right)^2}$ (e.g., Tvergaard and Hutchinson 1993), where δ_{slide} is the critical sliding displacement of the interface, and $\lambda = 1$ corresponds to complete interface debonding. The interface cohesive energy ϕ depends only on λ

$$\phi = \phi(\lambda). \tag{4}$$

For the interface cohesive law in Eq. 3, and a loading for λ increases from 0 towards 1, ϕ takes the form

$$\frac{\phi}{\gamma_{\text{int}}} = \begin{cases} \frac{1}{\lambda_e} \lambda^2 & \text{for stage-I, } \lambda \leq \lambda_e \\ 1 - \frac{1}{1-\lambda_e} (1-\lambda)^2 & \text{for stage-II, } \lambda_e < \lambda < 1. \\ 1 & \text{for stage-III, } \lambda \geq 1 \end{cases} \tag{5}$$

The normal and shear stresses at the particle/matrix interface are given by

$$\frac{\sigma^{\text{int}}}{\sigma_{\text{max}}} = \frac{\phi'(\lambda)}{2\gamma_{\text{int}}\lambda} \frac{[u]}{\delta_{\text{open}}} \tag{6}$$

$$\frac{\tau^{\text{int}}}{\tau_{\text{max}}} = \frac{\phi'(\lambda)}{2\gamma_{\text{int}}\lambda} \frac{[v]}{\delta_{\text{slide}}},$$

where $\tau_{\text{max}} = \frac{\delta_{\text{open}}}{\delta_{\text{slide}}} \sigma_{\text{max}}$.

For pure interface opening, Eq. 6 gives the same interface cohesive law as shown in Fig. 1 and Eq. 1. For pure interface sliding, Eq. 6 gives $\sigma^{\text{int}} = 0$ and

$$\frac{\tau^{\text{int}}}{\tau_{\text{max}}} = \begin{cases} \frac{1}{\lambda_e} \frac{[v]}{\delta_{\text{slide}}} & \text{for stage-I, } \frac{[v]}{\delta_{\text{slide}}} \leq \lambda_e \\ \frac{1}{1-\lambda_e} \left(1 - \frac{[v]}{\delta_{\text{slide}}} \right) & \text{for stage-II, } \lambda_e < \frac{[v]}{\delta_{\text{slide}}} < 1. \\ 0 & \text{for stage-III, } \frac{[v]}{\delta_{\text{slide}}} \geq 1 \end{cases} \tag{7}$$

The interface cohesive law for coupled opening and sliding involves four parameters, namely the critical opening displacement δ_{open} , the critical sliding displacement δ_{slide} , the linear modulus k and the softening modulus \tilde{k} . Currently we have determined three parameters, k, \tilde{k} and interface strength σ_{max} , for the particle/matrix interfaces in the high explosive PBX 9501. The critical opening displacement δ_{open} and the interface elastic limit λ_e relate to the measured three parameters through $\delta_{\text{open}} = \sigma_{\text{max}} \left(\frac{1}{k} + \frac{1}{\tilde{k}} \right)$ and $\lambda_e = \frac{\tilde{k}}{\tilde{k}+k}$, respectively. Another interface parameter, the critical sliding displacement δ_{slide} , remains unknown for the high explosive PBX 9501.

2.2 A fundamental solution

We first present a fundamental solution for the axisymmetric problem of an infinite matrix containing a spherical particle with radius a . As shown in Fig. 2, the matrix is subject to the remote axisymmetric stress $\sigma_{xx}^{\infty} = \sigma_{yy}^{\infty}$ and σ_{zz}^{∞} . The particle/matrix interface ($r = a$) has axisymmetric displacement discontinuities $[u]$ (opening displacement) and $[v]$ (sliding displacement) in the r and θ directions, respectively, where (r, θ, ψ) are the spherical coordinates centered at the particle. The general solution for an axisymmetric deformation field can always be expressed in terms of the Legendre polynomials $P_n(\cos \theta)$ (Lur e 1964). For example, the interface opening displacement $[u]$ and sliding displacement $[v]$, which depend only on θ , can be expressed as

$$[u] = \sum_{n=0}^{\infty} [u_n] P_n(\cos \theta) \tag{8}$$

$$[v] = \sum_{n=2}^{\infty} [v_n] P'_n(\cos \theta),$$

where the summation, here and thereafter, is for even numbers only, $P'_n(\cos \theta) = \frac{dP_n(\cos \theta)}{d\theta}$, and the coefficients $[u_n] = (2n + 1) \int_0^{\pi/2} [u] P_n(\cos \theta) \sin \theta d\theta$ and $[v_n] = \frac{2n+1}{n(n+1)} \int_0^{\pi/2} [v] P'_n(\cos \theta) \sin \theta d\theta$. The normal and shear stresses at the interface, σ^{int} and τ^{int} , can be similarly expressed as

$$\sigma^{\text{int}} = \sum_{n=0}^{\infty} \sigma_n^{\text{int}} P_n(\cos \theta) \tag{9}$$

$$\tau^{\text{int}} = \sum_{n=2}^{\infty} \tau_n^{\text{int}} P'_n(\cos \theta),$$

where the coefficients σ_n^{int} and τ_n^{int} are related to $[u_n]$ and $[v_n]$ by

$$\begin{aligned}
 &M_n^u \sigma_n^{\text{int}} + n(n+1) M_n^v \tau_n^{\text{int}} \\
 &= \frac{1 - \nu_m}{4(1 + \nu_m)\mu_m} (\sigma_{zz}^\infty + 2\sigma_{xx}^\infty) \delta_{n0} \\
 &\quad + \frac{5(1 - \nu_m)}{(7 - 5\nu_m)\mu_m} (\sigma_{zz}^\infty - \sigma_{xx}^\infty) \delta_{n2} - \frac{[u_n]}{a}, \\
 &M_n^v \sigma_n^{\text{int}} + (M_n^u + M_n^v) \tau_n^{\text{int}} \\
 &= \frac{5(1 - \nu_m)}{2(7 - 5\nu_m)\mu_m} (\sigma_{zz}^\infty - \sigma_{xx}^\infty) \delta_{n2} - \frac{[v_n]}{a}, \quad (10)
 \end{aligned}$$

where δ_{nm} is a Kronecker delta between integer m and n . Here

$$\begin{aligned}
 M_n^u &= \frac{2n^2 - 1 - (2n^2 - n - 2) \nu_p}{2(n-1)[n^2 + n + 1 + (2n+1)\nu_p] \mu_p} \\
 &\quad + \frac{2n^2 + 4n + 1 - (2n^2 + 5n + 1) \nu_m}{2(n+2)[n^2 + n + 1 - (2n+1)\nu_m] \mu_m} \\
 M_n^v &= \frac{2 - n + (2n - 1) \nu_p}{2(n-1)[n^2 + n + 1 + (2n+1)\nu_p] \mu_p} \\
 &\quad + \frac{n + 3 - (2n + 3) \nu_m}{2(n+2)[n^2 + n + 1 - (2n+1)\nu_m] \mu_m}, \quad (11)
 \end{aligned}$$

where μ_m (and ν_m) and μ_p (and ν_p) are shear moduli (and Poisson’s ratios) of the matrix and particles, respectively. Equation 10 gives two linear equations to solve σ_n^{int} and τ_n^{int} in terms of the remote stresses and displacement discontinuities across the particle/matrix interface. For the axial symmetrical problem considered in the fundamental solution, as shown in Fig. 2, the remote stress affects only modes $n = 0$ and 2 in Eq. 10.

For an interface with linear bonding, Eq. 10 gives

$$\sigma_n^{\text{int}} = \tau_n^{\text{int}} = 0, \quad \text{for } n > 2. \quad (12)$$

The interfacial tractions can then be written as

$$\begin{aligned}
 \sigma^{\text{int}} &= \sigma_0^{\text{int}} + \sigma_2^{\text{int}} \frac{3 \cos^2 \theta - 1}{2} \\
 \tau^{\text{int}} &= -3\tau_2^{\text{int}} \cos \theta \sin \theta,
 \end{aligned}$$

where σ_0^{int} , σ_2^{int} , and τ_2^{int} can be solved from Eq. 10. Therefore stress in the particle is uniform for linear interface bonding. Further, for perfect interface bonding the above derivation yields the same results where the Eshelby solution is typically used (Mura 1987). For interfaces with nonlinear debonding the statement in Eq. 12 does not apply, and the stress in the particle is non-uniform.

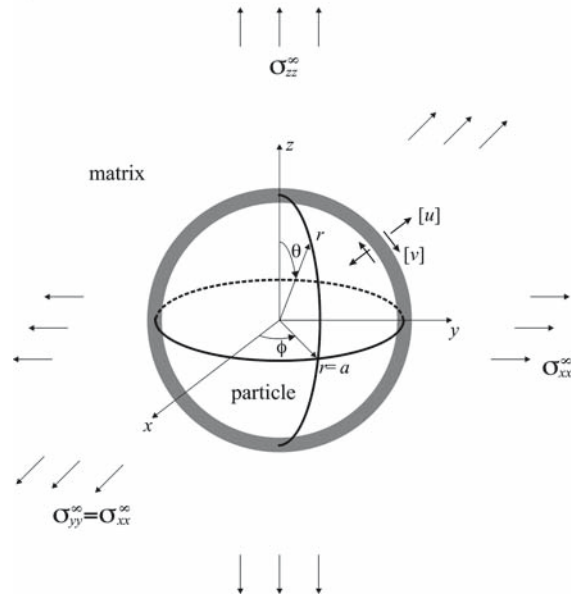


Fig. 2 An infinite matrix containing a spherical particle is subject to the remote axisymmetric stress

3 Extended Mori–Tanaka method accounting for particle/matrix interface debonding

The Mori–Tanaka method (Mori and Tanaka 1973) is extended in this section to account for the nonlinear interface debonding in the composite. The macroscopic stress $\bar{\sigma}$ and strain $\bar{\epsilon}$ represent the collective, homogenized behavior of the composite, and are uniform in the representative volume element. They are distinguished from their microscopic counterparts σ and ϵ in each constituent (particles and matrix), which are nonuniform due to material inhomogeneities, and satisfy the corresponding constitutive law for the constituent.

For a composite with particle volume fraction f subject to uniaxial tension along z direction, the relation between the axial stress $\bar{\sigma}_{zz}$ (denoted as $\bar{\sigma}$) and the axial strain $\bar{\epsilon}_{zz}$ (denoted as $\bar{\epsilon}$) is given by (e.g., Benveniste and Aboudi 1984; Tan et al. 2007)

$$\begin{aligned}
 \frac{\bar{\sigma}}{E_m} + f \left[\epsilon_{zz}^{\text{int}} + \left(\frac{1}{2\mu_p} - \frac{1}{2\mu_m} \right) \sigma_{zz}^p \right. \\
 \left. + \left(\frac{\nu_m}{E_m} - \frac{\nu_p}{E_p} \right) (\sigma_{xx}^p + \sigma_{yy}^p + \sigma_{zz}^p) \right] - \bar{\epsilon} = 0, \quad (13)
 \end{aligned}$$

where E_m and E_p are Young’s moduli of the matrix and particles, respectively; σ^p is the average stress in particles, and $\epsilon_{zz}^{\text{int}}$ is the additional strain due to interface

debonding, and is related to the displacement discontinuities $[u_z]$ across the particle/matrix interface S_{int} by

$$\varepsilon_{zz}^{\text{int}} = \frac{1}{\Omega_p} \int_{S_{\text{int}}} [u_z] n_z dA. \tag{14}$$

Here Ω_p is the particle volume and n_z is the component of the unit normal on the interface pointing into the matrix.

Particle sizes in the high explosive PBX 9501 show a bimodal distribution, with large and small particles debond simultaneously (Tan et al. 2005a, b, 2006). To simplify the problem for uniaxial loading, we consider a RVE with particles of the same size in this paper and assume that all the particles in the RVE debond to the same degree, i.e., $[u_n]$, $[v_n]$, σ_n^{int} , and τ_n^{int} are the same for all interfaces. As shown in the Appendix, the average stress in particles can be obtained in terms of the coefficients of Legendre polynomial coefficients σ_0^{int} , σ_2^{int} and τ_2^{int} in the fundamental solution in Sect. 2.2 as

$$\sigma_{zz}^p = \sigma_0^{\text{int}} + \frac{2}{5} (\sigma_2^{\text{int}} + 3\tau_2^{\text{int}}) \tag{15}$$

and

$$\sigma_{xx}^p + \sigma_{yy}^p + \sigma_{zz}^p = 3\sigma_0^{\text{int}}.$$

Similarly, the additional strain due to interface debonding is given in terms of $[u_n]$ and $[v_n]$ in the fundamental solution by

$$\varepsilon_{zz}^{\text{int}} = \frac{[u_0]}{a} + \frac{2([u_2] + 3[v_2])}{5a}. \tag{16}$$

The remote stress components, σ_{zz}^∞ and σ_{xx}^∞ , in the fundamental solution can be written as

$$\sigma_{zz}^\infty = \bar{\sigma} + \tilde{\sigma}_{zz} \tag{17}$$

$$\sigma_{xx}^\infty = \tilde{\sigma}_{xx},$$

where $\tilde{\sigma}_{xx}$ and $\tilde{\sigma}_{zz}$ are the average perturbed stresses in the matrix due to the presence of all inclusions (Weng 1984). The perturbed stresses relate to the average stresses in particles through

$$\tilde{\sigma}_{zz} = -\frac{f}{1-f} (\sigma_{zz}^p - \bar{\sigma}) \tag{18}$$

$$\tilde{\sigma}_{xx} = -\frac{f}{1-f} \sigma_{xx}^p.$$

With Eq. 15 the above equations become

$$\tilde{\sigma}_{zz} = -\frac{f}{1-f} \left[\sigma_0^{\text{int}} + \frac{2}{5} (\sigma_2^{\text{int}} + 3\tau_2^{\text{int}}) - \bar{\sigma} \right] \tag{19}$$

$$\tilde{\sigma}_{xx} = -\frac{f}{1-f} \left[\sigma_0^{\text{int}} - \frac{1}{5} (\sigma_2^{\text{int}} + 3\tau_2^{\text{int}}) \right].$$

Substituting the expressions for σ_{zz}^∞ and σ_{xx}^∞ into Eq. 10 gives σ_n^{int} and τ_n^{int} , relating to $[u_n]$ and $[v_n]$, as

$$\begin{aligned} & \left\{ M_n^u + \frac{f}{1-f} \left[\frac{3(1-\nu_m)}{4(1+\nu_m)\mu_m} \delta_{n0} + \frac{3(1-\nu_m)}{(7-5\nu_m)\mu_m} \delta_{n2} \right] \right\} \sigma_n^{\text{int}} \\ & + \left[n(n+1) M_n^v + \frac{f}{1-f} \frac{9(1-\nu_m)}{(7-5\nu_m)\mu_m} \delta_{n2} \right] \tau_n^{\text{int}} \\ & = \frac{1}{1-f} \left[\frac{1-\nu_m}{4(1+\nu_m)\mu_m} \delta_{n0} + \frac{5(1-\nu_m)}{(7-5\nu_m)\mu_m} \delta_{n2} \right] \bar{\sigma} - \frac{[u_n]}{a} \end{aligned}$$

and

$$\begin{aligned} & \left[M_n^v + \frac{f}{1-f} \frac{3(1-\nu_m)}{2(7-5\nu_m)\mu_m} \delta_{n2} \right] \sigma_n^{\text{int}} \\ & + \left[M_n^u + M_n^v + \frac{f}{1-f} \frac{9(1-\nu_m)}{2(7-5\nu_m)\mu_m} \delta_{n2} \right] \tau_n^{\text{int}} \\ & = \frac{1}{1-f} \frac{5(1-\nu_m)}{2(7-5\nu_m)\mu_m} \delta_{n2} \bar{\sigma} - \frac{[v_n]}{a}. \end{aligned} \tag{20}$$

Therefore, only $[u_n]$ and $[v_n]$ remain to be determined, and they can be obtained by minimizing the total potential energy density of the RVE Π , which is a functional of $[u]$ and $[v]$, through

$$\delta \Pi ([u], [v]) = 0. \tag{21}$$

The total potential energy density of the RVE, $\Pi ([u], [v])$, is a sum of the elastic strain energy density U and the potential energy of the macroscopic stress $\bar{\sigma}$. For a RVE with controlled macroscopic strain $\bar{\varepsilon}$ (during the variation of interfacial jumps $[u]$ and $[v]$), the variation of the potential energy of the macroscopic stress $\bar{\sigma}$ is zero. Therefore,

$$\delta \Pi ([u], [v]) = \delta U ([u], [v]) = 0. \tag{22}$$

Here the elastic energy density of the RVE, U , consists of the energy $\int_{S_{\text{int}}} \phi dA$ due to interface debonding and the strain energy in the matrix and particles. For a RVE subject to uniaxial tension, the strain energy density U is given for any micromechanics model (e.g., dilute solution, Mori–Tanaka method) as

$$\begin{aligned} U = \frac{1}{2} \bar{\sigma} \bar{\varepsilon} + \frac{3f}{a} \left\{ \int_0^{\pi/2} \phi \sin \theta d\theta \right. \\ \left. - \sum_{n=0}^{\infty} \frac{\sigma_n^{\text{int}} [u_n] + n(n+1) \tau_n^{\text{int}} [v_n]}{2(2n+1)} \right\}, \end{aligned} \tag{23}$$

where ϕ is a nonlinear function of $[u_n]$ and $[v_n]$ obtained from Eqs. 3–5. Using the relations (14)–(17) for the Mori–Tanaka method, the above strain energy density can be written in terms of $[u_n]$ and $[v_n]$ as

$$\begin{aligned}
U = & \frac{\bar{\sigma}^2}{2E_0} - \frac{3f}{a^2} \left\{ \frac{1 - K_m/K_0}{1 - K_m/K_p} \frac{[u_0]^2}{2M_0^u} \right. \\
& \left. + \frac{1 - \mu_m/\mu_0}{1 - \mu_m/\mu_p} \frac{([u_2] + 3[v_2])^2}{25(M_2^u + 3M_2^v)} \right\} \\
& + \frac{3f}{a} \int_0^{\pi/2} \phi \sin \theta d\theta \\
& + \frac{3f}{2a^2} \sum_{n=0}^{\infty} \frac{(M_n^u + M_n^v) [u_n]^2 - 2n(n+1) M_n^v [u_n][v_n] + n(n+1) M_n^u [v_n]^2}{(2n+1) [M_n^u + (n+1) M_n^v] (M_n^u - n M_n^v)}, \quad (24)
\end{aligned}$$

where

$$\begin{aligned}
\bar{\sigma} = E_0 \left(\bar{\varepsilon} - \frac{1 - K_m/K_0}{1 - K_m/K_p} \frac{[u_0]}{a} \right. \\
\left. - \frac{1 - \mu_m/\mu_0}{1 - \mu_m/\mu_p} \frac{2[u_2] + 6[v_2]}{5a} \right). \quad (25)
\end{aligned}$$

Here E_0 , K_0 and μ_0 are respectively the Young's, bulk and shear moduli given by the Mori–Tanaka method for a composite without interface debonding ($[u] = [v] = 0$), and are given in the Appendix.

According to Eq. 22, the Legendre components of the interface displacement discontinuity, $[u_n]$ and $[v_n]$, can be obtained from

$$\begin{aligned}
\frac{\partial U}{\partial [u_n]} &= 0 \\
\frac{\partial U}{\partial [v_n]} &= 0. \quad (26)
\end{aligned}$$

Once $[u_n]$ and $[v_n]$ are obtained from Eqs. (26) for a composite subject to uniaxial strain $\bar{\varepsilon}$, we can use $[u_0]$, $[u_2]$, and $[v_2]$ to construct the stress–strain relation of the composite using Eq. 25. It is interesting to notice that Eq. 25 is identical to that for the dilute solution (Tan et al. 2007) if E_0 , K_0 and μ_0 are substituted by their corresponding expressions in the dilute solution.

The interface cohesive law enters into the Mori–Tanaka method through Eq. 24, where the strain energy density U of the composite material contains the energy $\int_{S_{\text{int}}} \phi dA$ due to interface debonding. The difference between the Mori–Tanaka method and the dilute method in dealing with the constitutive behaviors of composite materials accounting for the nonlinear interface debonding is that: in dilute solution, the remote stress σ^∞ in the fundamental solution is taken as the applied composite stress $\bar{\sigma}$ (Tan et al. 2007); while in the Mori–Tanaka method, the remote stress σ^∞ is taken as the average stress σ^m in the matrix. Through this way interactions between particles are considered in

the Mori–Tanaka method. The method can therefore be applied to investigate behaviors of solid propellants and high explosives, where the particle volume fraction is high and the interactions between particles can not be neglected.

4 Results

The material properties are taken from the high explosive PBX 9501. The elastic bulk and shear moduli of particles are $K_p = 12.5$ GPa and $\mu_p = 5.43$ GPa (Zaug 1998). The matrix Young's modulus is $E_m = 1$ MPa, and Poisson's ratio $\nu_m = 0.499$ (Cady et al. 2006; Mas et al. 2001). The interface cohesive law for the high explosive PBX 9501 has the cohesive strength $\sigma_{\text{max}} = 1.66$ MPa, linear modulus $k = 1.55$ GPa/ μm and softening modulus $\tilde{k} = 17$ MPa/mm (Tan et al. 2005b), which give the critical opening displacement $\delta_{\text{open}} = 98$ μm .

4.1 Particle volume fraction f

Figure 3 shows the macroscopic stress–strain curves of the composite (solid curves) with particle volume fraction $f = 10\%$, 60% , and 93% , where 93% is the particle volume fraction in the high explosive PBX 9501 that contains large particles (radius $a = 125$ μm) and small particles (radius $a = 4$ μm). The tensile stress $\bar{\sigma}$ is normalized by the interface cohesive strength σ_{max} . The particle radius is fixed at $a = 125$ μm , which is the radius of large particles in the PBX 9501. The critical sliding displacement is the same as the critical opening displacement, i.e., $\delta_{\text{slide}} = \delta_{\text{open}}$. Figure 3 also shows the stress–strain curves of the composite predicted from a non-cohesive model (dashed lines), where interface displacements are assumed to be zero. However, interface displacements are not zero when the interface is in linear debonding stage. Therefore, Fig. 3 reflects the significant effect of interface debonding on the Young's modulus. For each particle volume fraction, the curve for interface debonding is clearly lower than that without debonding.

As the particle volume fraction increases, the Young's modulus (initial slope of the stress–strain

curve) increases sharply because the elastic modulus of particles (~ 10 GPa) is several orders of magnitude higher than that of the matrix (~ 1 MPa). The particle volume fraction also affects the strength (peak stress) of the composite, which is 1.04 times the interface cohesive strength, $1.04\sigma_{\max}$, for $f = 93\%$ and $0.89\sigma_{\max}$ and $0.62\sigma_{\max}$ for $f = 60\%$ and 10% , respectively. Once the peak stress is reached, the stress–strain curve reaches the softening stage. For $f = 10\%$, the stress–strain curve shows an abrupt drop after the peak stress, i.e., the so called the “catastrophic debonding” (Tan et al. 2007). For high particle volume fraction ($f = 60\%$ and 93%), the abrupt drop disappears and the stress–strain curves displays gradual decrease after the peak. This is consistent with the analytical solution for the composite with interface debonding subject to hydrostatic tension (Tan et al. 2005a).

The curve for $f = 60\%$ in Fig. 3 becomes lower than that for $f = 10\%$ at the large strain. This is because, at the large strain, the debonded particles become effectively the voids. A higher particle volume fraction then gives a higher void volume fraction, and therefore lower stress–strain curve.

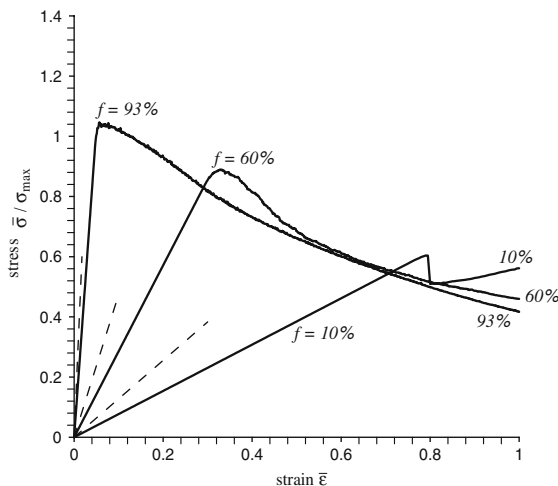


Fig. 3 The stress–strain curves for particle volume fraction $f = 10\%$, 60% , and 93% , where the stress is normalized by the interface cohesive strength σ_{\max} . The particle radius is $125 \mu\text{m}$, and the critical sliding displacement is the same as the critical opening displacement, $\delta_{\text{slide}} = \delta_{\text{open}}$. The stress–strain curves predicted from a non-cohesive model are also shown

4.2 Particle size a

The solid lines in Fig. 4 show the normalized stress, $\bar{\sigma} / \sigma_{\max}$, versus the strain for small particle radius $a = 4 \mu\text{m}$ and large particle radius $a = 125 \mu\text{m}$, respectively. These two particle sizes are used in the high explosive PBX 9501 (Skidmore et al. 1997; Berghout et al. 2002). The particle volume fraction is $f = 60\%$, and the critical sliding and opening displacements are the same, $\delta_{\text{slide}} = \delta_{\text{open}}$. Small particles ($a = 4 \mu\text{m}$) give the hardening behavior, while large particles ($a = 125 \mu\text{m}$) lead to softening behavior. This particle size effect has also been observed in the dilute solution (Tan et al. 2007), and therefore holds for both low and high particle volume fractions.

It is interesting to point out that it is always the particle radius a times interface cohesive zone moduli, k for linear debonding and \tilde{k} for softening, that is compared with the moduli of particles and the matrix (see also Tan et al. 2007). Classical micromechanics models are size independent. The particle radius a enters into the formulation of the composite energy density U through in two places: one is in the fundamental solution as

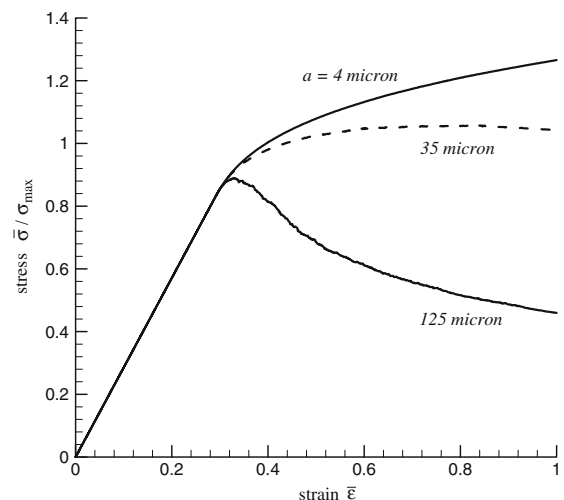


Fig. 4 The stress–strain curves for particle radius $a = 4, 35,$ and $125 \mu\text{m}$, where the stress is normalized by the interface cohesive strength σ_{\max} . The particle volume fraction is $f = 60\%$, and the critical sliding displacement is the same as the critical opening displacement, $\delta_{\text{slide}} = \delta_{\text{open}}$

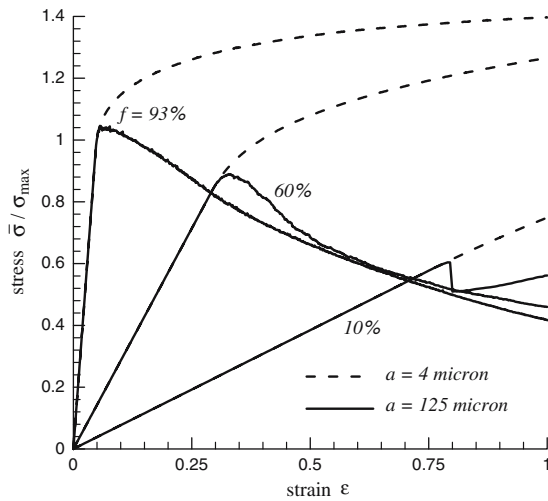


Fig. 5 Particle size effect at different volume fraction $f = 10\%$, 60% , and 93% . The solid lines give the stress–strain curves for large particles with radius $125\ \mu\text{m}$, while the dashed lines for small particles with radius $4\ \mu\text{m}$. The stress is normalized by the interface cohesive strength σ_{max} . The critical sliding displacement is the same as the critical opening displacement, $\delta_{\text{slide}} = \delta_{\text{open}}$

given in Eq. 10; the other is through the specific surface $3f/a$, which is the interface area per unit volume of the material, as given in Eq. 24.

The reason for the large and small particles to display different behavior (at the same particle volume fraction) is that the contribution from interface debonding to the tangent modulus is $-\tilde{k}a$. For large particle radius, $\tilde{k}a$ may overwhelm the Young's modulus E_0 (for composite without interface debonding) such that the increment modulus becomes negative, i.e., softening.

There exists a critical part size that separates the hardening and softening behaviors, and it is about $35\ \mu\text{m}$ for the present material properties, as shown by the dashed line in Fig. 4. This corresponds to the ratio of particle radius to critical opening displacement $a/\delta_{\text{open}} = 0.36$. This particle size effect clearly results from the length scale introduced in the interface cohesive law. The micromechanics models that do not account for interface debonding can only predict size-independent material behavior.

Figure 5 further shows the particle size effect at different volume fraction $f = 10\%$, 60% , and 93% . The dashed line is for particle size $a = 4\ \mu\text{m}$, and solid line for $a = 125\ \mu\text{m}$. The results indicate that: for the composites with material parameters specified in the

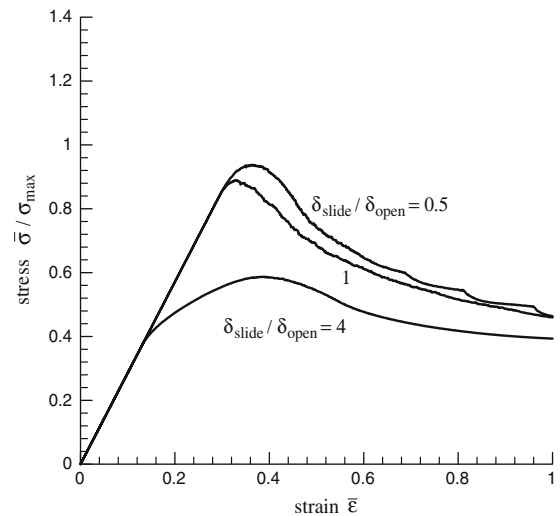


Fig. 6 The stress–strain curves for critical sliding displacement $\delta_{\text{slide}} = 0.5, 1$, and 4 times the critical opening displacement δ_{open} , where the stress is normalized by the interface cohesive strength σ_{max} . The particle volume fraction is $f = 60\%$, and the particle radius $a = 125\ \mu\text{m}$

beginning of the section the constitutive behaviors always show hardening for small particles with radius of $4\ \mu\text{m}$.

4.3 Interface sliding

Figure 6 shows the normalized stress, $\bar{\sigma}/\sigma_{\text{max}}$, versus the strain for different ratio of critical sliding to opening displacements, $\delta_{\text{slide}}/\delta_{\text{open}} = 0.5, 1$, and 4 . The particle radius is $a = 125\ \mu\text{m}$, and the particle volume fraction is $f = 60\%$. All curves have the same initial slope. For small critical sliding displacement $\delta_{\text{slide}} = 0.5\delta_{\text{open}}$, the peak stress as well as the stress–strain curve are higher than their counterparts for $\delta_{\text{slide}} = \delta_{\text{open}}$ and $4\delta_{\text{open}}$. This suggests that interface sliding may significantly affect the stress–strain behavior of the composite. In fact, δ_{slide} should be determined from experiments that involve significant shear, such as uniaxial tension.

5 Conclusions and Discussions

We have used a nonlinear cohesive law for particle/matrix interfaces to study the effect of interface debond-

ing on the macroscopic behavior of particle-reinforced composite materials subject to uniaxial tension. The Mori–Tanaka method, which is suitable for composite with high particle volume fraction, is extended to account for interface debonding. At a fixed particle volume fraction, small particles lead to hardening behavior of the composite while large particles yield softening behavior. The interface sliding may contribute significantly to the macroscopic behavior of the composite.

The interface debonding $[u]$ between the large particles and the matrix in PBX 9501 is around 100 micron (Tan et al. 2005b). The contribution of interface debonding to the composite strain is on the order of $[u]/a$, where a is the average radius of particles. For large particles in PBX 9501 the radius a is around 125 microns (Skidmore et al. 1997), so $[u]/a$ is close to 100%. In the Figs. 3–6, the average strains are plotted to values of one, corresponding to 100% strain. Such large strains mostly occur through interface debonding.

Acknowledgements This research was supported by the U.S. Department of Energy and the U.S. Department of Defense/Office of Land Warfare & Munitions under the Joint DoD/DOE Munitions Technology Development Program, ONR Composites for Marine Structures Program (grants N00014-01-1-0205, Program Manager Dr. Y. D. S. Rajapakse), and the Midwest Structural Sciences Center (MSSC) supported by the U.S. Air Force Research Laboratory Air Vehicles Directorate under contract number FA8650-06-2-3620.

Appendix

The average stress in the particle is $\sigma_{ij}^p = \frac{1}{\Omega_p} \int_{\Omega_p} \sigma_{ij} dV = \frac{1}{\Omega_p} \int_{\Omega_p} \sigma_{ik} \delta_{jk} dV = \frac{1}{\Omega_p} \int_{\Omega_p} \sigma_{ik} x_{j,k} dV = \frac{1}{\Omega_p} \int_{\Omega_p} (\sigma_{ik} x_j)_{,k} dV = \frac{1}{\Omega_p} \int_{S_{int}} \sigma_{ik} x_j n_k dA$, where the equilibrium equation $\sigma_{ik,k} = 0$ and divergence theorem have been used. It is noted that is the stress traction, i.e., σ^{int} and τ^{int} in r and θ directions, respectively. The substitution of σ^{int} and τ^{int} in Eq. 9 into the above integral gives the average stress in particles in Eq. 14.

The average strain ε_{zz}^{int} due to interface debonding can be similarly obtained by substituting $[u]$ and $[v]$ in Eq. 8 into Eq. 13, where $[u_z] = [u] \cos \theta - [v] \sin \theta$.

The Mori–Tanaka solution gives the bulk and shear moduli of a composite without interface debonding as $K_0 = K_m \left[1 + \frac{f \left(\frac{K_p}{K_m} - 1 \right)}{1 + (1-f) \frac{1+\nu_m}{3(1-\nu_m)} \left(\frac{K_p}{K_m} - 1 \right)} \right]$ and

$$\mu_0 = \mu_m \left[1 + \frac{f \left(\frac{\mu_p}{\mu_m} - 1 \right)}{1 + (1-f) \frac{2(4-5\nu_m)}{15(1-\nu_m)} \left(\frac{\mu_p}{\mu_m} - 1 \right)} \right].$$

The Young’s modulus is given by $E_0 = \frac{9\mu_0 K_0}{\mu_0 + 3K_0}$.

References

Benveniste Y, Aboudi J (1984) A continuum model for fiber reinforced materials with debonding. *Int J Solids Struct* 20:935–951

Berghout HL, Son SF, Skidmore CB, Idar DJ, Asay BW (2002) Combustion of damaged PBX 9501 explosive. *Thermochim Acta* 384:261–277

Cady CM, Blumenthal WR, Gray DJ III (2006) Mechanical properties of plastic-bonded explosive binder materials as a function of strain-rate and temperature. *Polym Eng Sci* 46:812–819

Camacho GT, Ortiz M (1996) Computational modelling of impact damage in brittle materials. *Int J Solids Struct* 33:2899–2938

Espinosa HD, Zavattieri PD, Dwivedi SK (1998) A finite deformation continuum/discrete model for the description of fragmentation and damage in brittle materials. *J Mech Phys Solids* 46:1909–1942

Geubelle PH, Baylor JS (1998) Impact-induced delamination of composites: a 2D simulation. *Compos B* 29:589–602

Huang Y, Gao H (2001) Intersonic crack propagation. Part I: the fundamental solution. *J Appl Mech* 68:169–175

Kubair DV, Geubelle PH, Huang Y (2002) Intersonic crack propagation in homogeneous media under shear-dominated loading: theoretical analysis. *J Mech Phys Solids* 50:1547–1564

Kubair DV, Geubelle PH, Huang Y (2003) Analysis of a rate-dependent cohesive model for dynamic crack propagation. *Eng Fract Mech* 50:685–704

Lur  AI (1964) Three-dimensional problems of the theory of elasticity. Interscience Publishers, New York

Mas EM, Clements BE, Blumenthal WR, Cady CM, Gray GT III, Liu C (2001) A viscoelastic model for PBX binders. In: Furnish MD, Thadhani NN, Horie Y (eds) Proceedings of 2001 conference of the APS topical group on shock compression of condensed matter, American Institute of Physics, Woodbury, New York

Mori T, Tanaka K (1973) Average stress in matrix and average elastic energy of materials with misfitting inclusions. *Acta Metall* 21:571–574

Mura T (1987) Micromechanics of defects in solids. Martinus Nijhoff Publishers, Dordrecht

Needleman A (1987) A continuum model for void nucleation by inclusion debonding. *J Appl Mech* 54:525–531

Samudrala O, Huang Y, Rosakis AJ (2002) Subsonic and intersonic mode II crack propagation with a rate-dependent cohesive zone. *J Mech Phys Solids* 50:1231–1268

Samudrala O, Rosakis AJ (2003) Effect of loading and geometry on the subsonic/inter-sonic transition of a bimaterial interface crack. *Eng Fract Mech* 70:309–337

Skidmore CB, Phillips DS, Son SF, Asay BW (1997) Characterization of HMX particles in PBX 9501. In: Proceedings of the topical conference on shock compression of condensed

- matter, Los Alamos, New Mexico, American Institute of Physics, pp 112–119
- Tan H, Huang Y, Liu C, Geubelle PH (2005a) The Mori–Tanaka method for composite materials with nonlinear interface debonding. *Int J Plasticity* 21:1890–1918
- Tan H, Liu C, Huang Y, Geubelle PH (2005b) The cohesive law for the particle/matrix interfaces in high explosives. *J Mech Phys Solids* 53:1892–1917
- Tan H, Huang Y, Liu C, Geubelle PH (2006) Effect of nonlinear interface debonding on the constitutive model of composite materials. *Int J Multiscale Comput Eng* 4:147–167
- Tan H, Huang Y, Liu C, Ravichandran G, Inglis HM, Geubelle PH (2007) The uniaxial tension of particle-reinforced composite materials with nonlinear interface debonding. *Int J Solids Struct* 44:1809–1822
- Thiagarajan G, Hsia KJ, Huang Y (2004a) Finite element implementation of Virtual Internal Bond model for crack behavior simulation. *Eng Fract Mech* 71:401–423
- Thiagarajan G, Huang Y, Hsia KJ (2004b) Fracture simulation using an elasto-viscoplastic virtual internal bond model with finite elements. *J Appl Mech* 71:796–804
- Tvergaard V, Hutchinson JW (1992) The relation between crack growth resistance and fracture process parameters in elastic-plastic solids. *J Mech Phys Solids* 40:1377–1397
- Tvergaard V, Hutchinson JW (1993) The influence of plasticity on mixed-mode interface toughness. *J Mech Phys Solids* 41:1119–1135
- Weng GJ (1984) Some elastic properties of reinforced solids, with special reference to isotropic ones containing spherical inclusions. *Int J Eng Sci* 22:845–856
- Xu XP, Needleman A (1994) Numerical simulations of fast crack growth in brittle solids. *J Mech Phys Solids* 42:1397–1434
- Zaug JM (1998) Elastic constants of β -HMX and tantalum, equations of state of supercritical fluids and fluid mixtures and thermal transport determinations. In: *Proceedings of 11th international detonation symposium, Snowmass, Colorado*, p 498
- Zhang P, Klein PA, Huang Y, Gao H, Wu PD (2002) Numerical simulation of cohesive fracture by the Virtual-Internal-Bond model. *Comput Modeling Eng Sci* 3:263–278
- Zhong XA, Knauss WG (1997) Analysis of interfacial failure in particle-filled elastomers. *J Eng Mater Technol* 119:198–204
- Zhong XA, Knauss WG (1999) On the stability of phase separation in a finite solid with interfaces. *Mech Compos Mater Struct* 6:1–7
- Zhong XA, Knauss WG (2000) Effects of particle interaction and size variation on damage evolution in filled elastomers. *Mech Comput Mater Struct* 7:35–53